



An experimental investigation of the effects of diode laser surface hardening of AISI 410 stainless steel and comparison with furnace hardening heat treatment

Mahmoud Moradi^{1,2} · Hossein Arabi^{1,2} · Alexander F. H. Kaplan³

Received: 7 January 2019 / Accepted: 3 September 2019 / Published online: 17 September 2019
© The Brazilian Society of Mechanical Sciences and Engineering 2019

Abstract

This study investigated the ability of the continuous wave diode laser surface hardening of AISI 410 martensitic stainless steel with a maximum power of 1600 W. Variable process parameters scanning speed (4–7 mm/s), laser power (1200–1600 W) and stand-off distance (65–75 mm) were considered in this study. Microhardness, the geometry of hardened layer (depth and width), microhardness deviation from the base metal microhardness (MHD), microstructure analysis of the laser-hardened zone through optical microscopy and field emission scanning electron microscopy and percentage of the ferrite phase in AISI 410 microstructure by using Clemex software were considered as process output responses. Results confirmed that by increasing the laser power and reducing the scanning speed, the surface hardness and the depth of hardness increase. It is also revealed the width of the hardened area increases by enhancing stand-off distance and reducing the laser power. Maximum hardness of 630 HV0.3 with 2.2 mm depth is obtained. Also, the furnace hardening heat treatment is compared with the laser hardening process. Microstructure, microhardness, and impact tests of the two processes are compared. Results showed that the hardness of the diode laser is 1.4 times the hardness of the furnace hardening heat treatment.

Keywords Laser surface hardening · Diode laser · Microhardness · AISI 410 martensitic stainless steel · Microhardness deviation

1 Introduction

To improve surface properties of materials, especially steels, which are widely used in industry, traditional heat treatment methods are very popular, but modern methods like laser

surface treatment are more precise [1]. Laser processing is used for various applications such as laser welding, brazing, and hardening [2–7], laser drilling [8], and laser cutting [9]. The diode lasers are one of the most used and advanced lasers in the modern industry. This type of laser with high accuracy heat-treated the surface of the matter. Martensitic stainless steels are used in several industries including petroleum, gas and petrochemical, food, and pharmaceutical. These alloys are used in manufacturing corrosion resistance pipes and plates and applied in an acidic environment which are more economical than similar grades [10]. One type of martensitic stainless steels widely used in industry is AISI 410 from 400 series of these steels. Surface hardening is one of the laser surface treatment processes in which the laser is selected with preset parameters. These parameters are variables dependent on the type of laser and material to be treated. After selecting optimum parameters, laser hardening accomplishes, and surface hardness of steel improves which transformation of ferrite and austenite phase to martensite will lead to more hardness [11]. Mahmoodi et al. [12] carried out laser surface treatment of AISI 420 by means of

Technical Editor: Lincoln Cardoso Brandao.

✉ Mahmoud Moradi
moradi.malayeru@gmail.com
Hossein Arabi
arabi8252@gmail.com
Alexander F. H. Kaplan
alexander.kaplan@ltu.se

- ¹ Department of Mechanical Engineering, Faculty of Engineering, Malayer University, P.O. Box 65719-95863, Malayer, Iran
- ² Laser Materials Processing Research Centre, Malayer University, Malayer, Iran
- ³ Department of Engineering Sciences and Mathematics, Lulea University of Technology, 971 87 Luleå, Sweden

Nd:YAG laser in pulsed module, in which microhardness in the depth and width of hardened area was studied. To compare the ability of CO₂ laser and diode laser in hardening of AISI 1045, Li et al. [13] investigated the effect of each process on quality of the surface hardening. According to experimental data of laser hardening by these two types of lasers, they simulated the process, which showed the quality achieved by high-power diode laser was higher than the one by CO₂ laser. Guarino et al. [14] used a high-power diode laser to develop the fatigue life of AISI 1040 steel. Results revealed that laser treatment could considerably increase the fatigue life. Netprasert et al. [15] studied to harden the AISI 420 martensitic stainless steel by using a nanosecond pulse laser. The results showed that the microhardness increased from 242 to 1700 HV and the depth of the hardened layer was created to be 60–80 μm. Yazici et al. [16] investigated the effect of different processing temperatures on wear properties of high-power diode laser on R260 grade rail steel. Martinez et al. [17] surveyed the effects of the distinctly applied laser heat treatment (LHT) and ultrasonic impact treatment (UIT) and the joined LHT + UIT process on the wear and friction behaviors of the hardened surface layers of the tool steel AISI D2. Syed et al. [18] studied effects of surface hardening by using a high-power diode laser on C–Mn low-carbon automotive steel. Barka et al. [19] investigated a simulating model (finite difference method) and experimental method for laser hardening of 4340 steel. Telasang et al. [20] investigated properties of corrosion resistance and wear of AISI H13 steel, which hardened up to 800 Vickers. Idan et al. [21] compared the effects of CO₂ laser hardening and tempering of 40, 40Cr and 38Cr2MoAl steels in GOST Russian standard. Saftar et al. [22] investigated the effects of beam geometries (circular, inverse triangle, rectangular beams) by using high-power diode laser on the laser surface hardening process. Moradi et al. [23] studied laser surface hardening of AISI 410 by using a 700 W Nd:YAG laser in which the effect of laser pulse energy and focal point position on geometrical dimensions and microhardness of hardened zone was investigated. Jahromi et al. [24] investigated a study by Nd:YAG laser on the three different microstructures of AISI 410 martensitic stainless steel samples heat-treated including: fine ferrite, fine and coarse martensite. Furthermore, finite element simulation was done using ABAQUS software to predict diffusion on the hardness of the different microstructures by using Nd:YAG laser. A mathematical model for Nd:YAG laser surface hardening of 42CrMo steel was presented by using finite element method and verified by experimental results by Sun et al. [25]. Ehlers et al. [26] carried out laser surface hardening of AISI 4140 steel sheet by using a 2000 W diode laser. The maximum hardness reached 740 HV with 1.9 mm depth in this study.

In spite of the efforts of these and other researchers, investigation on diode laser hardening of AISI 410 martensitic

stainless steel has not survived before. The use of diode lasers to increase the depth and width of hardness, as well as hardness uniformity in the hardened area, is considered as an effective challenge in other lasers, including the Nd:YAG laser, which was previously written by the authors of this paper. In this study, the effect of laser power, scanning speed and the stand-off distance (SOD) on the surface hardness and geometrical dimensions of the hardened area of AISI 410 was studied by using diode laser. The microstructure changes of the steel surface were also measured and investigated. The microstructure of the hardened area was evaluated. Also, the microstructural and mechanical properties of furnace heat treatment were compared with the diode laser surface hardening. Figure 1 depicts the cross-section and geometrical responses of the hardened zone. The microstructure of the hardened area was surveyed by OM and FESEM devices. MHD and the percentage of the ferrite phase in the structure were investigated.

2 Experimental work

The chemical composition of AISI 410 stainless steel used in this research is mentioned in Table 1. The chemical composition was measured by atomic spectroscopy. The specimens width (specifications of the thickness = 10 mm and the diameter = 65 mm) were selected.

In Fig. 2, the mechanism of the laser surface hardening process is depicted schematically. The laser stand-off distance or focal plane position is also shown in Fig. 2.

A diode laser with a maximum power of 1600 W was used as a heat source for this research. Experimental settings and outcomes of laser hardening process by diode laser are shown in Table 2. Scanning speed (4–7 mm/s), laser power (1200–1600 W), and stand-off distance (65–75 mm) were considered as input variables. Table 3 shows the different dimensions of the incidence beam with a different focal plane position used in this research.



Fig. 1 Specimen cross-section and geometrical responses of the hardened zone

Table 1 Chemical composition (wt%) of AISI 410

Element name	C	Mo	Cr	Cu	S	P	Mn	Ni	Si	Al	V	Fe
Weight percent	0.15	0.03	13.5	0.11	0.024	0.018	0.51	0.12	0.28	0.008	0.021	Balance

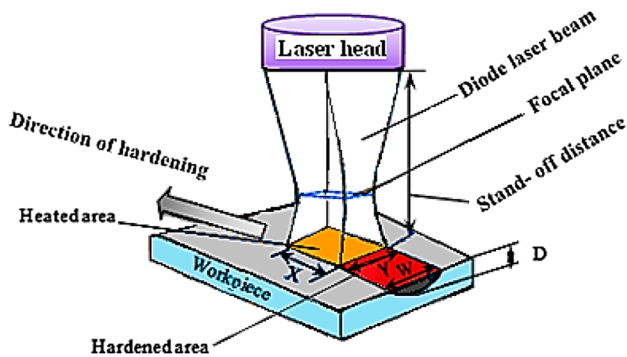


Fig. 2 The schematic mechanism of the laser hardening process

In Fig. 3, images of AISI 410 samples hardened by diode laser are shown. To investigate the microstructure of the hardened area, the samples are firstly cut into specific pieces, and by mounting and metallurgical preparations they have been etched in the villa’s reagent with a formula of (Hcl 5 cc, C6H3N3O7 2 gr, C2H5OH 100 cc). Then, OM and FESEM images are taken. Microhardness was accomplished by a micro-indentation device with a maximum load of 300 gr and a dwell time of 30 s. The geometric dimensions (depth and width) of the hardened area were obtained. Figure 1 shows the depth and width of hardness as a macroscopic structure. The Precision measurement of hardened dimensions was done by ImageJ software. Figure 4 illustrates the cross-sectional view of Vickers indenters in the depth and width of the hardened layer. The interval of the points in the depth and width is 100 μm and 300 μm, respectively.

Table 3 The relationship between the incident beam length, width, and area

Stand-off distance (mm)	Incident beam length (x) (mm)	Incident beam width (y) (mm)	Incident beam area (x-y) (mm ²)
65	2.55	9.94	25.34
70	3.60	11.88	42.77
75	4.65	13.82	64.30

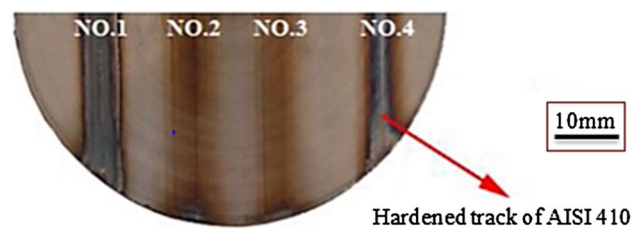


Fig. 3 Image of the hardened laser samples (sample diameter is 65 mm)

3 Results and discussion

In this research, the effects of diode laser parameters (i.e., scanning speed, laser power, and stand-off distance) on AISI 410 martensitic stainless steel in surface hardening process were studied. To investigate the metallurgical properties, geometrical dimensions of the hardened area, microhardness distribution of the laser hardening, microstructure on the hardened surface, MHD and the percentage of the ferrite phase in the structure were analyzed.

Table 2 Experimental layout and outcomes

Sample number	Input parameters			Output results					
	Scanning speed (mm/s)	Stand-off distance (mm)	Laser power (W)	Maximum hardness (HV)	The depth of hardness (mm)	The width of hardness (mm)	MHD in depth	MHD in width	Ferrite percent (%)
1	5	65	1400	630	2.2	8.12	18,813.71	28,651.62	0.52
2	6	70	1200	490	1.4	8.42	12,399.23	16,417.13	1.92
3	4	70	1200	540	1.7	8.33	16,211.64	21,364.23	0.71
4	6	70	1600	620	1.8	8.21	18,658.42	26,621.61	0.62
5	7	65	1400	530	1.6	8.41	16,053.43	20,813.71	1.10
6	5	75	1400	520	1.5	8.52	15,311.97	18,355.25	1.50

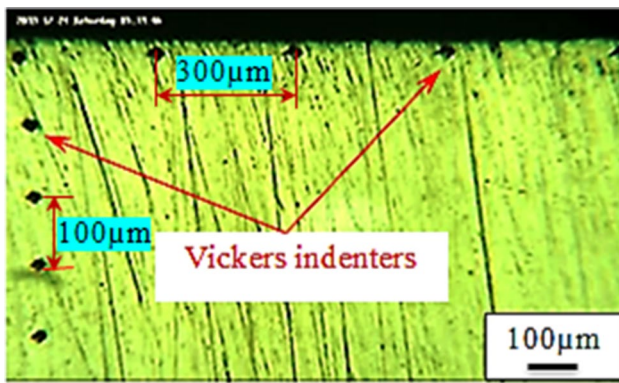


Fig. 4 Image of Vickers indenters

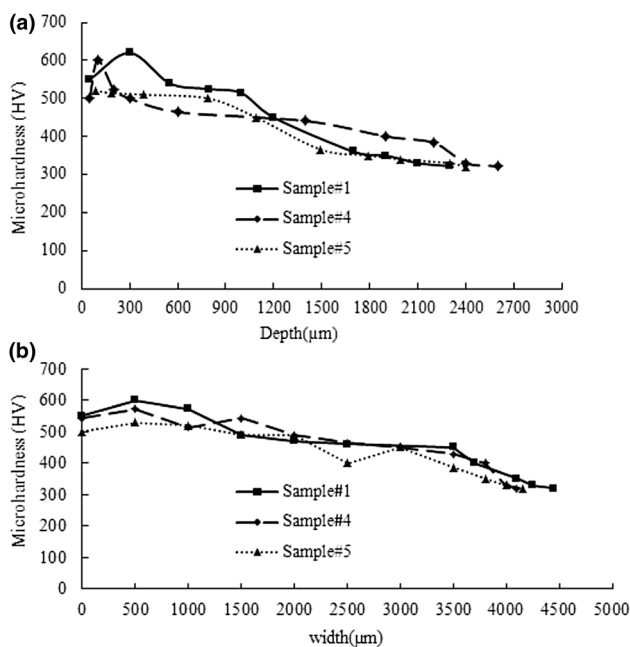
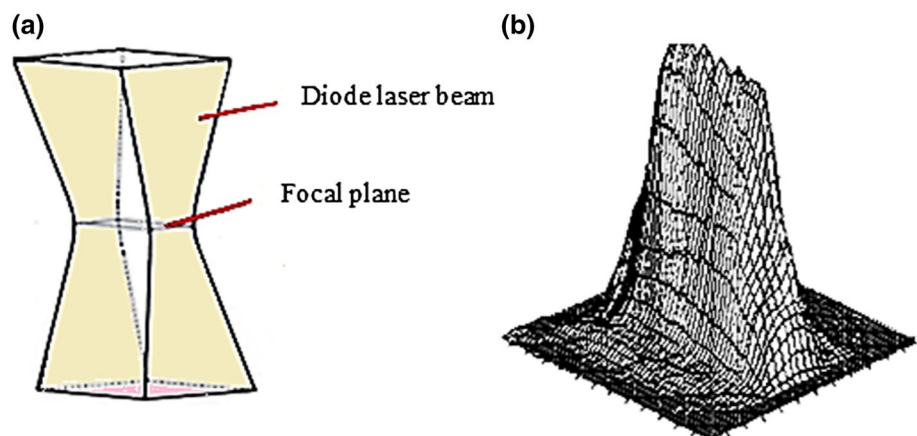


Fig. 5 Microhardness profile of the hardened layer in **a** depth and **b** width

Fig. 6 **a** Distribution of the diode laser beam energy, **b** the shape of top-hat energy distribution [27, 28]



3.1 Microhardness distribution

Figure 5a, b shows the microhardness changes from the surface to the depth and width of samples 1, 4 and 5.

In Fig. 5a, it is clear that surface hardness is increased and little by little is decreased along the depth of the hardened zone to reach the base metal hardness. It is because of the reduction in transferred laser energy in the material. Fine grain martensitic and ferrite phase dispersed in the hardened area. It is because of the high rate of quenching during laser hardening process, which produces unique metallurgical effects in the steel, such as improvement in microstructure and grain size and higher hardness with appropriate toughness in the steel. Figure 5b depicts the microhardness distribution of the hardened layer in width. It is displayed in half of the width of the hardened zone. As it is clear, its distribution is like a sinusoidal function that in the hardness is the maximum in the center and decreases gradually in the outside of the hardened area. The reason for this phenomenon is the rectangular energy distribution of the laser beam that is illustrated in Fig. 6.

Figure 6a, b depicts the images of the energy distribution in the diode laser beam and the shape of top-hat energy distribution, respectively [27]. Maximum surface hardness occurs in sample number 1 equal to 630 HV0.3 hardness. It means that the surface hardness increases 90% from 330 HV of the base metal.

To improve the results of the laser hardening process, the following parameters should be carefully considered:

1. The amount of heat entering the laser beam to the surface of the material.
2. The effect of metallurgical factors on the microstructure of the hardened area, such as grain size.

At first, the effect of heat input on the workpiece surface is studied. Equation 1 shows the laser heat input to the surface [29].

$$H = P/S \quad (1)$$

Therefore, by increasing the power of the laser beam and reducing the scanning speed on the workpiece, the heat input increases. Increases in the heat input lead to increases in the hardness, while for sample #1, sample #4, and sample #5 the heat input is 280 (J/mm), 266.6 (J/mm), and 200 (J/mm), respectively. The grain size of the laser-hardened zone is an important issue for considering. The ASTM-112 standard is used to measure the grain size. To specify the grain size, the usual heat treatment cycle should be initiated at 850 °C for 1 h and then cooled at the furnace temperature. After achieving the declared heat treatment with a suitable etching solution, the initial austenite particle, which is a solid solution of carbon and is stable at high temperatures, is studied. Indeed, by measuring the size of the initial austenite, by using the Nital solution (2 ml nitric acid and 98 ml ethanol alcohol) the grain size is estimated [30]. For the base metal of the AISI 410, ASTM grain size number = 7 (Equal to 30 μm) reach to ASTM grain size number = 11 (Equal to 7 μm). By reducing the size of the initial austenitic grains, the structure is susceptible to the formation of a smaller martensitic phase during the process of austenite transformation into martensite. As the particle size of the martensite increases, the hardness of the surface of the hardened area increases. The Hall–Petch equation [30, 31] presents the relationship between the size of the grain in the microstructural and mechanical properties. Equation 2 describes Hall–Petch relation:

$$\sigma_0 = \sigma_i + KD^{-1/2} \quad (2)$$

where σ_i is yield stress, σ_0 is the friction stress, K is the locking parameter, and D is the mean diameter of the grain. Due to reduced grain size, the strength of the material and mechanical properties improve.

3.2 Geometrical dimensions of the hardened layer

As it is discussed above for Fig. 6, the shape of the geometrical dimensions of the hardened zone is similar to the form of the laser energy distribution. By increasing the stand-off distance, the laser beam diverges, and the energy density is decreased, and a spot diameter of the laser becomes larger. In this paper, increasing the stand-off distance (SOD) means getting away from the focal plane which is affected by the penetration depth and also the hardness. Figure 7a illustrates the effect of SOD on the distribution of the hardness in the depth of the hardened zone. It is shown that in sample #1 (SOD=65 mm) the trend of hardness is higher than sample #6 (SOD=75 mm). The reason is that decreasing the distance between the spot plane of the laser and workpiece causes more energy induced in metal. It leads to an increase in the metallurgical transformation and causes more

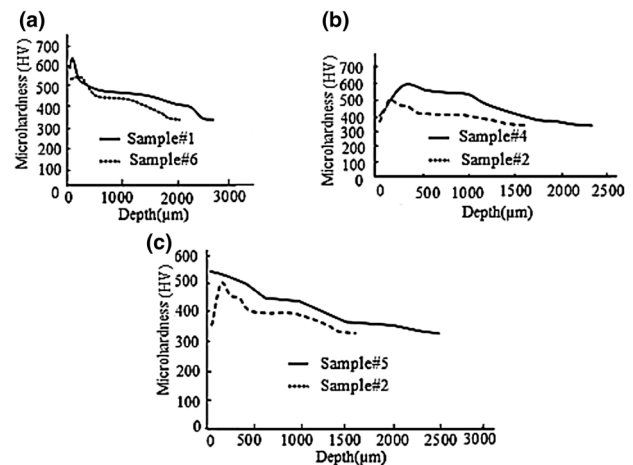


Fig. 7 Image of microhardness profile for depth of the hardened area, **a** effect of stand-off distance, **b** effect of laser power, **c** effect of scanning speed

hardness. By focusing on the results presented in Table 2, it can understand that increasing the laser power causes increases in the depth of the hardened layer. More laser power leads to the increase in the austenitic temperature. So the microhardness and geometrical dimensions increase (compare samples #4 and samples #2). Figure 7b illustrates the influence of the laser power on the hardness distribution in the depth of the hardened layer. Scanning speed has a direct effect on the laser hardening results. Decreasing scanning speed increases the interaction time between the laser beam and the workpiece. Therefore, heat input energy to the material increases which leads to the increase in the hardness and geometrical dimensions of the hardened layer.

Influence of scanning speed could be seen in sample #5 and samples #2 (see Table 2). Figure 7c illustrates the influence of scanning speed on the hardness distribution in the depth of the hardened layer. In the following discussion, the influence of three other important parameters that have an important influence on the geometric dimensions is presented. These parameters are beam density of the diode laser, the shape of the distribution of energy beam in diode laser, and metallurgical properties such as the form of the phases in the microstructure, which are described below. The energy beam density of the diode laser is shown in Eq. 3 [3].

$$\text{Beam density} = \text{Laser power} / \text{Incident beam area} \quad (3)$$

By increasing the density of the energy beam, the surface temperature of the workpiece increases. Then the austenitic temperature rises, so hardness and the depth of the hardened area are increased. Tables 2 and 3 present the incident beam area and the laser power. By using Eq. 3, the beam density is calculated, for sample #1 and sample #6 as shown in Fig. 7a, which is 55.25 W/mm² and 21.77 W/mm², respectively. Therefore, with more beam density in sample

#1, the geometric dimensions (depth and width) of the hardened area will be greater. According to Fig. 7b, the beam density of sample #4 and sample #2 is 37.40 W/mm^2 and 28.05 W/mm^2 , respectively. The reason for the increase in the geometric dimensions (of the hardened area) in sample #4, compared to the sample #2, is the increase in the beam density of sample #4. In Fig. 7c, both sample #5 and sample #2 have the same beam density, but because of increasing the heat input in sample #5 than sample #2 the geometric dimensions will be increased.

As shown in Fig. 6, the form of the energy distribution in the diode laser is rectangular. This top-hat distribution of energy leads to the expansion of the heat affected area, and the hardened area becomes larger, so the geometric dimensions of the hardened area are larger than another laser beams that are in the form of a Gaussian distribution, such as Nd:YAG laser and fiber laser. In addition, when the shape of the particles is extended in the microstructure, the thermal conductivity and laser penetration increase, so the geometric dimensions of the hardened area increase. What concluded from the microstructure images is that ferrite particles are stretched; therefore, the penetration of the thermal energy of diode laser in the depth and width of the workpiece increases.

3.3 Microstructure of hardened layer

To study the effect of laser hardening process on the microstructure of the material, the metallographic survey is performed by using optical microscopy (OM) and field emission scanning electron microscopy (FESEM). Figure 8a, b shows the microstructure of AISI 410 raw material by using OM and FESEM, respectively. It is seen that in its raw material ferrite is distributed in the martensitic field. It is obvious that there are several ferrite particles in the martensitic field.

Investigations show that when the heat input energy of the laser increases (lower scanning speed, higher laser power, and lower SOD), austenite temperature for transformation phase increases and austenite grains become finer. Therefore, in this case, the ferrite phase percent decreases. By controlling the scanning speed, grains could be uniform. Figure 9a, b shows the microstructure of hardened layer of AISI 410 by using optical microscopy. It is observed that the figure of the ferrite is extended and becomes finer in the microstructure. Consequently, in the laser hardening process by a diode laser, the hardness and geometric dimensions (depth and width) increase.

Figure 10a, b illustrates the microstructure of the hardened layer of sample #1 and sample #4, respectively. These images are taken by using the FESEM. Due to higher laser energy, martensitic particles are finer, and ferrite particles are dissolved in the structure fields. Therefore, laser hardening has caused the higher surface hardness, more uniform and suitable

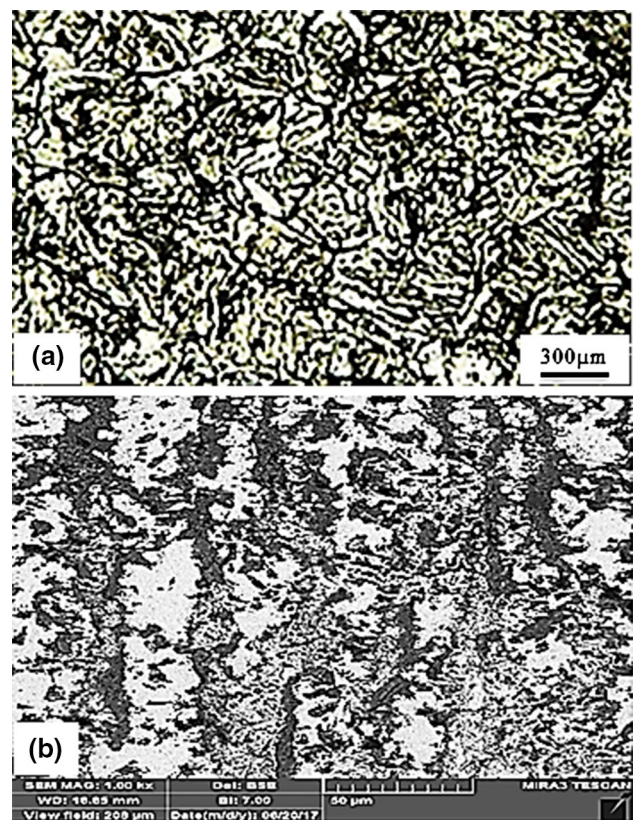


Fig. 8 Microstructure of AISI 410 raw material, a OM, b FESEM

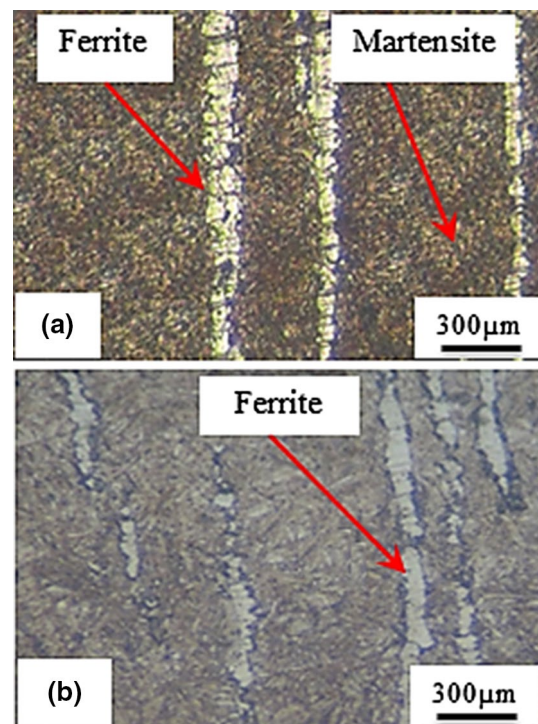


Fig. 9 The microstructure of AISI 410 laser-hardened layer (OM), a sample #1, b sample #4

Fig. 10 The microstructure of AISI 410 laser-hardened layer (FESEM), a sample #1, b sample #4

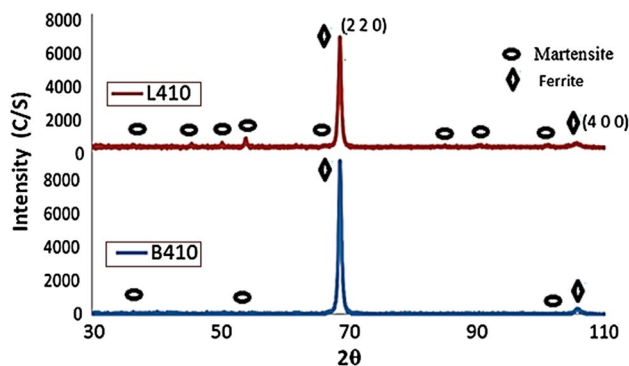
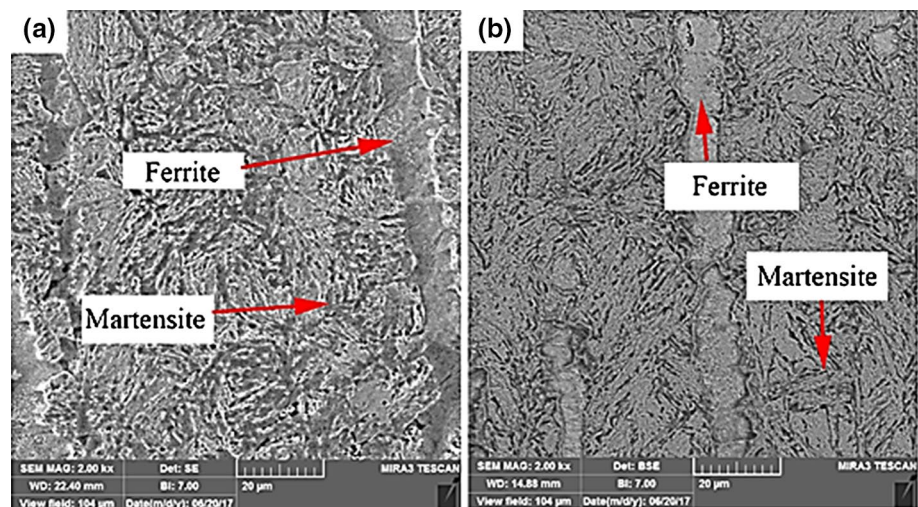


Fig. 11 XRD spectra in the raw material (B410) and after the laser hardening (L410)

structure. It is observed that the ferrites are stretched and martensites are stretched and needle-shaped in the structure. Thus, laser hardening caused major changes in the size of the martensitic phase and the dissolution of the ferrites.

XRD spectra of raw material and laser-hardened area are shown in Fig. 11. By considering the XRD spectra, the martensite and ferrite phases are visible. Also, the ferrite and martensite particles of AISI 410 are smaller than raw material. Thus, XRD spectra confirm the hardness and geometric dimensions in the hardened area increase.

3.4 Microhardness deviation from the base metal (MHD)

To study how the microhardness distribution profile changes at the depth and width of the hardened area, the parameter of MHD is used according to Eq. 4 [32].

$$\text{MHD} = \sum_{i=1}^n \frac{(X_i - X_{b,m})^2}{n} \quad (4)$$

where X_i is the microhardness of point i and $X_{b,m}$ is raw metal microhardness, and n is the number of measured microhardness points. In the present research, n is 10 and $X_{b,m}$ is equal to 330 wickers for AISI 410 stainless steel. The higher MHD in the laser hardening is more desirable. MHD is one of the most important output parameters in this study. Indeed, MHD designates the uniformity of hardness in the hardened area.

3.5 The percentage of the ferrite phase

By analyzing images of the microstructure using Clemex software, the amount of ferrite phase particles in the structure of the hardened samples was obtained. The results are presented in Table 2. The existence of ferrite in the hardened area reduces the hardness and strength of the steel. Microstructure images of the hardened surface were selected along the center of the hardened area. In Fig. 12a, b the red dots represent the ferrite phase and the blue field indicate martensites. As shown in Table 2, in Fig. 12a, the percentage of ferrite is lower than that of Fig. 12b, The reason is that sample number #1 has a higher heat input energy (higher laser power and lower stand-off distance). Thus by increasing the laser thermal energy, the steel's austenitic temperature rises and the ferrites phases are solved in the structure. Figure 13 depicts the relationship of ferrite percentage with the maximum surface hardness of samples. As seen, decreasing the ferrite percentage results in the increase in the maximum surface hardness.

3.6 Comparison of the furnace hardening heat treatment (FHHT) and diode laser hardening (DLH)

In this section, FHHT was conducted to compare with the DLH method. For comparing the DLH with the conventional method, the furnace heat treatment according

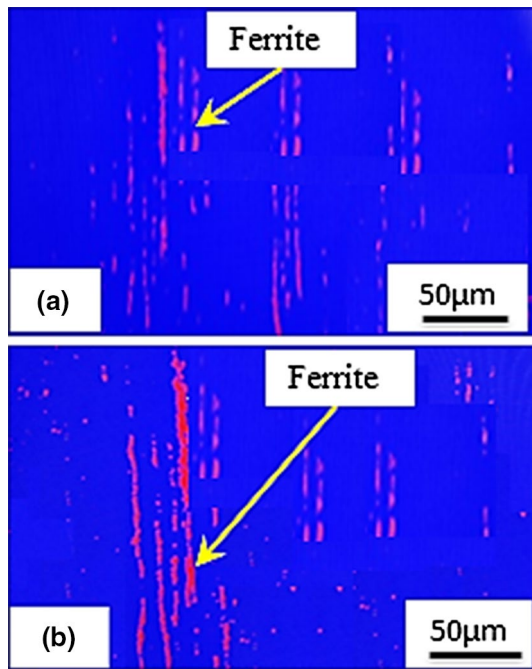


Fig. 12 Determination of ferrite percentage by Clemex software a sample #1, b sample #2

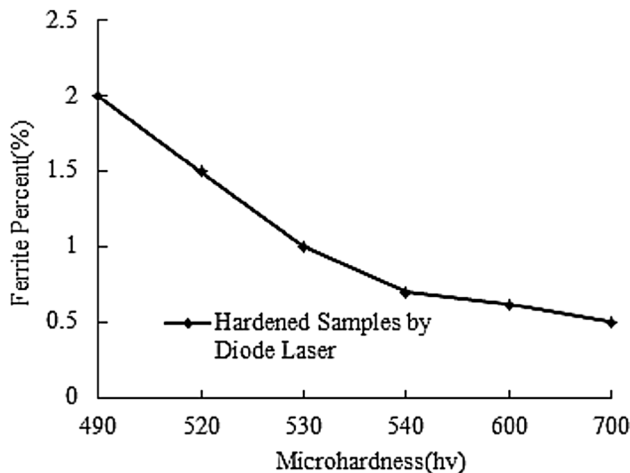


Fig. 13 Profile of ferrite percent in microhardness

to the cycle presented in Fig. 14 was performed. The AISI 410 samples preheated to 540 °C for 1 h, heated to 980 °C with the rate of 70 °C/h, and were kept for 2 h. Then samples were quenched with three ways (air, oil, and water-cooling).

3.6.1 Comparison of the hardness

Table 4 shows the comparison of the hardness results of furnace hardening heat treatment and laser surface hardening.

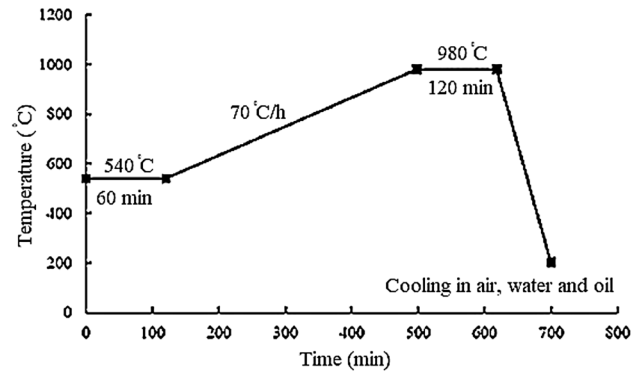


Fig. 14 Image of FHHT cycle for AISI 410 stainless steel [33]

Table 4 Comparison of furnace hardening heat treatment and laser hardening

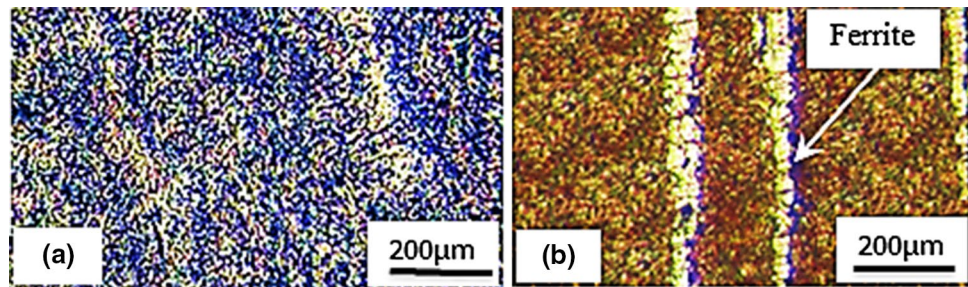
Heat treatment cycle	Furnace hardening heat treatment	Laser hardening
Cooling in oil	434 Vickers	–
Cooling in water	446 Vickers	–
Cooling in air	412 Vickers	–
Self-cooling (self-quenching)	–	630 Vickers

As seen in Table 4, the hardness of furnace hardened of AISI 410 stainless steel quenched in the air, oil, and water is 412 Vickers, 434 Vickers, and 446 Vickers, respectively. Due to the possibility of microcrack formation in the water, and the lower the hardness in the air, the oil is an ideal quenching method with a hardness of 434 Vickers for AISI 410. So the hardness value with the diode laser hardening method (630 Vickers) is 1.4 times than the furnace hardening heat treatment.

3.6.2 Comparison of the microstructure

As shown in Fig. 15a, b the fine ferrites are dispersed in the rough martensitic field of FHHT samples, while in the DLH, these elements are interconnected in the fine martensitic field. Due to the high-energy concentration in the DLH, local hardness occurs, while in the FHHT, the hardness is volumetric. The existence of ferrite in the martensite field reduces the hardness and strength of the steel. Because of small interaction time in the laser and high speed of the process, ferrites are detected in the martensite field. To reduce or remove them, increasing the laser power and slowing down the scanning speed could overcome this challenge. In FHHT technique, because of keeping the sample at a specific time during the heating cycle, in the microstructure, fine ferrite and rough martensite phases are observed. Hence, in the

Fig. 15 Microstructure images of the hardened sample **a** FHHT, oil-quenched **b** DLH, sample #1



FHHT technique the hardness increases, but this structure is brittle.

3.6.3 Comparison of the impact test and fracture toughness

According to the heat treatment cycle of Fig. 14, AISI 410 is heated to 980 °C; at this temperature, the microstructure consists of austenite and ferrite; then, with the quenching operation, the sample is rapidly cooled, and the martensitic and ferrite particles are obtained with a very tough structure. Quenching operation creates internal stresses as well as brittle structures in steel. In this process, the hardness of the steel is higher, but the mechanical properties are reduced. To improve the mechanical properties of steel, such as an increase in toughness and a reduction in the residual stress after the quenching operation, the tempering heat treatment cycle is performed. The temperature and time selection of tempering operations depends on the chemical composition of the steel, and the dimensions of the pieces and the mechanical properties are required. Tempering is performed by controlled heating of the quenched workpiece called the lower transformation temperature (under the temperature of 723 °C). This steel conducted relatively high hardness and strength after tempering at such high temperature of 600–700 °C [28]. In the present study, to investigate the hardness and toughness of the furnace heat treatment hardening samples, tempering the sample with high temperatures of 650 °C, tempering the sample with a minimum of 250 °C [33], and not tempering the sample, compared to the laser-hardened sample, were accomplished. Toughness properties by impact test (according to ASTM-A370 standard

at ambient temperature) and microstructure analysis have been evaluated. Charpy impact tests at ambient temperature and amount of energy absorbed by studied structures with dimensions of 10 mm × 10 mm × 55 mm and with V-notch to a depth of 2 mm during fracture were conducted (see Table 5). The results showed that hardness of the samples at 250 °C and 650 °C reached 412 HV and 380 HV, respectively. In addition, the results of the impact test on the furnace heat treatment samples at the tempering setup of 250 °C and 650 °C reached 12 J and 22 J, respectively. Thus, in furnace heat treatment samples, if the tempering operation is carried out at 650 °C, the hardness will be reduced to 380 HV, while the toughness will be better. By tempering operation at 250 °C, the hardness will reach 412 HV, but the steel will be quite brittle. The impact test was also performed on the best laser surface hardening sample of AISI 410 (sample #1).

About the impact energy values, Eq. 5 describes the fracture toughness [34]:

$$K_{IC}^2 = 0.22E \times (CVN)^{1.5} \quad (5)$$

where k_{1c} is the fracture toughness in the plane strain states, E is Young's modulus, and CVN is the impact energy of the V-notch sample in the Charpy impact test, and fracture toughness is a property, which describes the ability of a material to resist fracture and is one of the most important properties of any material for many design applications. Fracture toughness is a quantitative way of expressing a material's resistance to brittle fracture when a crack is present. A material with high fracture toughness may undergo ductile fracture as opposed to brittle fracture. According

Table 5 Comparison of the hardness and impact test at 25 °C (ambient temperature) and fracture toughness of the FHHT and DLH methods

Type of operation	Base metal	Furnace heat treatment, oil-quenched without tempering operation	Furnace heat treatment, oil-quenched with tempering operation at 250 °C	Furnace heat treatment, oil-quenched with tempering operation at 650 °C	Diode laser hardening by self-quenching
Hardness (HV)	336	434	412	380	630
Impact energy (J)	15	10	12	22	35
Fracture toughness k_{1c} (MP√m)	51.31	37.85	43.40	68.38	96.87

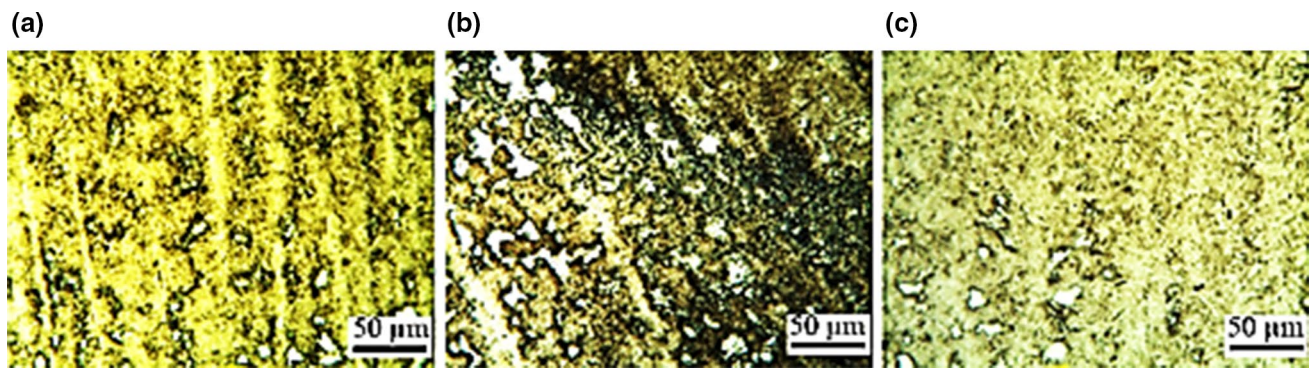


Fig. 16 Microstructure images of the tempering operation at **a** 250 °C, **b** 650 °C, **c** diode laser hardening

to Table 5, the result shows that diode laser hardening has higher hardness and toughness than furnace hardening heat treatment. Having a higher hardness and higher fracture toughness at the same time in laser surface hardening could improve the application of this process, which could have so many applications in industries such as steam turbine blade application. Figure 16a, b and c shows images of the microstructure of tempering operation at 250 °C and 650 °C and diode laser hardening, respectively. Fine particles of ferrite and martensite exist in the structure of the tempered at 250 °C, which causes the higher hardness and the lower fracture toughness (see Fig. 16a). As shown in Fig. 16b, in the tempered state at 650 °C, the coarse ferrite and martensite particles has been scattered in the microstructure, this can be lead to lower hardness and higher fracture toughness in the AISI 410 hardened sample. In the diode laser hardening, as shown in Fig. 16c, finer particles of ferrite and martensite can be seen which causes the higher hardness and the higher fracture toughness.

4 Conclusions

The influences of diode laser parameters (i.e., laser power, scanning speed, and stand-off distance) on AISI 410 martensitic stainless steel in surface transformation hardening process were studied. Geometrical dimensions of the hardened layer, microhardness distribution in the depth and width of laser hardening, and microstructure on the hardened surface were analyzed. The following conclusions can be drawn:

1. Increasing the laser power and reducing scanning speed (increasing heat input) lead to increases in microhardness and depth of the hardened layer. Decreasing the stand-off distance causes more energy induced to the material. Regarding rectangular energy distribution of

the laser beam, hardness and depth of the hardening layer increase.

2. The maximum surface hardness of 630 HV0.3 with the maximum depth of the hardened layer of 2.2 mm is obtained. It means that the surface hardness increases 90% from 330 HV of the base metal.
3. The microhardness deviation (MHD) specifies the uniformity of hardness in the hardened area, so, if the hardness decreases gradually from surface to depth, the MHD in the depth will be higher.
4. To reduce or eliminate ferrite phases, the lower scanning speed and the higher laser power are recommended. Also in the laser hardening, ferrite particles are interconnected in the microstructure. However, in the furnace hardening operation, are finer and more dispersed.
5. The hardness value of the diode laser hardening method (630 HV0.3) is 1.4 times that of furnace hardening heat treatment.
6. The maximum hardness and impact energy values for the laser-hardened samples are 630 HV and 35 J, respectively, while these values for the furnace heat treatment sample are 380 HV and 35 J, respectively.

References

1. Kannatey Asibu E Jr (2009) Principles of laser materials processing, 2nd edn. Wiley, NJ, pp 568–581
2. Moradi M, Karami Moghadam M, Kazazi M (2019) Improved laser surface hardening of AISI 4130 low alloy steel with electrophoretically deposited carbon coating. *Optik* 178(February):614–622
3. Moradi M, Karami Moghadam M (2019) High power diode laser surface hardening of AISI 4130; statistical modeling and optimization. *Opt Laser Technol* 111(April):554–570
4. Khorram A, Jafari A, Moradi M (2018) Effect of linear heat input on the morphology and mechanical properties of Ti–6Al–4V welded using a CO₂ laser. *Lasers Eng* 40(1–3):49–64

5. Faraji AH, Moradi M, Goodarzi M, Colucci P, Maletta C (2017) An investigation on the capability of hybrid Nd:YAG laser-TIG welding technology for AA2198 Al–Li alloy. *Opt Lasers Eng* 96:1–6
6. Khorram A, Jafari A, Moradi M (2017) Laser brazing of 321 and 410 stainless steels using BNI-2 nickel-based filler metal. *Modares Mech Eng* 17(1):129–135
7. Moradi M, Ghoreishi M, Khorram A (2018) Process and outcome comparison between laser, tungsten inert gas (TIG) and laser-TIG hybrid welding. *J Lasers Eng* 39(3–6):379–391
8. Moradi M, Mohazabpak A (2018) Statistical modeling and optimization of laser percussion micro-drilling on Inconel 718 sheet using response surface methodology. *J Lasers Eng* 39(4–6):313–331
9. Moradi M, Mehrabi O, Azdast T, Benyounis KY (2017) Enhancement of low power CO₂ laser cutting process for injection molded polycarbonate. *Opt Laser Technol* 96C:208–218
10. Li L (2000) The advances and characteristics of high-power diode laser materials processing. *Opt Lasers Eng* 34:231–253
11. Puli R, Janaki Ram GD (2012) Wear and corrosion performance of AISI 410 martensitic stainless steel coatings produced using friction surfacing and manual metal arc welding. *Surf Coat Technol* 209(24):1–7
12. Mahmoudi B, Sabour Aghdam AR, Torkamany MJ (2010) Controlled laser transformation hardening of martensitic stainless steel by pulsed Nd: YAG laser. *Electron Sci Technol* 8(01):87–90
13. Li R, Jin Y, Li Zh, Qi K (2014) A comparative study of high-power diode laser and CO₂ laser surface hardening of AISI 1045 steel. *Mater Eng Perform* 23(09):3085–3091
14. Guarino S, Barletta M, Afilal A (2017) High power diode laser (HPDL) surface hardening of low carbon steel: Fatigue life improvement analysis. *J Manuf Process* 28(01):266–271
15. Netprasert O, Tangwarodomnukun V, Dumkum Ch (2018) Surface hardening of AISI 420 stainless steel by using a nanosecond pulse laser. *Mater Sci Forum* 911:44–48
16. Yazici O, Yilmaz S (2018) Investigation of effect of various processing temperatures on abrasive wear behaviour of high power diode laser treated R260 grade rail steels. *Tribol Int* 119:222–229
17. Lesyk DA, Martinez S, Mordyuk BN, Dzhemelinskiy VV, Lamikiz A, Prokopenko GI, Grinkevych KE, Tkachenko IV (2018) Laser-hardened and ultrasonically peened surface layers on tool steel AISI D2: correlation of the bearing curves' parameters, hardness and wear. *J Mater Eng Perform* 27(02):764–776
18. Syed B, Shariff SM, Padmanabham G, Lenka Sh, Bhattacharya B, Kundu S (2017) Influence of laser surface hardened layer on mechanical properties of re-engineered low carbon steel sheet. *Mater Sci Eng A* 685:168–177
19. Barka N, Brousseau J (2018) Case study of laser hardening process applied to 4340 steel cylindrical specimens using simulation and experimental validation. *Case Stud Therm Eng* 11:15–25
20. Telasang G, Majumdar JD, Padmanabham G, Manna I (2015) Wear and corrosion behavior of laser surface engineered AISI H13 hot-working tool steel. *Surf Coat Technol* 261(01):69–78
21. Idan AFI, Akimov O, Golovco L, Goncharuk O, Kostyk K (2016) The study of the influence of laser hardening conditions on the change in properties of steel. *Iadn* 2(5):69–73
22. Safdar Sh, Li L, Sheikh MA, Schmidt MJ (2004) Modelling the effect of laser beam geometry on laser surface heating of metallic materials. In: *Proceedings of the 23 international congress on applications of lasers and electro-optics*
23. Moradi M, KaramiMoghadam M, Zarei J, Ganji B (2017) The effects of gha laser pulse energy and focal point position on laser surface hardening of AISI 410 stainless steel. *Modares Mech Eng* 17(7):311–318
24. Jenabali Jahromi SA, Khajeh A, Mahmoudi B (2012) Effect of different pre-heat treatment processes on the hardness of AISI 410 martensitic stainless steels surface-treated using pulsed neodymium-doped yttrium aluminum garnet laser. *Mater Des* 34:857–862
25. Sun P, Li Sh, Yu G, He X, Zheng C, Ning W (2014) Laser surface hardening of 42CrMo cast steel for obtaining a wide and uniform hardened layer by shaped beams. *Int J Adv Manuf Technol* 70:787–796
26. Ehlers B, Herfurth HJ, Heinemann S (2000) Hardening and welding with high power diode lasers. *Proc SPIE* 3945:63–70
27. Li R, Jin Y, Li Zh, Qi K (2014) A comparative study of high-power diode laser and CO₂ laser surface hardening of AISI 1045 steel. *JMEPEG* 23:3085–3091
28. Moradi M, Fallah MM, Jamshidi Nasab S (2018) Experimental study of surface hardening of AISI 420 martensitic stainless steel using high power diode laser. *Trans Indian Inst Metal* 71(8):2043–2050
29. Haddadi E, Moradi M, Karimzad Ghavidel A, Karimzad Ghavidel A, Meiabadi S (2019) Experimental and parametric evaluation of cut quality characteristics in CO₂ laser cutting of polystyrene. *Optik* 184:103–114
30. Jung B, Lee H, Park H (2013) Effect of grain size on the indentation hardness for polycrystalline materials by the modified strain gradient theory. *Int J Solids Struct* 50:2719–2724
31. Liu X, Yuan F, Wei Y (2013) Grain size effect on the hardness of nanocrystal measured by the nano-size indenter. *Appl Surf Sci* 279:159–166
32. Jelokhani-Niaraki MR, Mostafa Arab NB, Naffakh-Moosavy H, Ghoreishi M (2016) The systematic parameter optimization in the Nd:YAG laser beam welding of Inconel 625. *Int J Adv Manuf Technol* 84(9–12):2537–2546
33. Moradi M, Arabi H, Jamshidi Nasab S, Benyounis KY (2019) A comparative study of laser surface hardening of AISI 410 and 420 martensitic stainless steels by using diode laser. *Opt Laser Technol* 111:347–357
34. Salemi Golezani A (2013) The effect of microstructure on estimation of the fracture toughness (KIC) rotor steel using charpy absorbed energy (CVN). *J Adv Mater Process* 1(3):11–17

Publisher's Note Springer Nature remains neutral with regard to jurisdictional claims in published maps and institutional affiliations.